Taylor & Francis
Taylor & Francis Group

REPORT

🔓 OPEN ACCESS   Ⓜ Check for updates

Quality comparability assessment of a SARS-CoV-2-neutralizing antibody across transient, mini-pool-derived and single-clone CHO cells

Gangling Xu[a,#], Chuanfei Yu[a,#], Wenbo Wang[a,#], Cexiong Fu[b], Hongchuan Liu[b], Yanping Zhu[b], Yuan Li[b], Chunyu Liu[a], Zhihao Fu[a], Gang Wu[a], Meng Li[a], Sha Guo[a], Xiaojuan Yu[a], Jialiang Du[a], Yalan Yang[a], Maoqin Duan[a], Yongfei Cui[a], Hui Feng[b], and Lan Wang[a]

aKey Laboratory of the Ministry of Health for Research on Quality and Standardization of Biotech Products, China National Institutes for Food and Drug Control, Beijing, China; bShanghai Junshi Biosciences Co. Ltd, Shanghai, China

ABSTRACT

The emergence of severe acute respiratory syndrome coronavirus 2 (SARS-CoV-2) has triggered a serious public health crisis worldwide, and considering the novelty of the disease, preventative and therapeutic measures alike are urgently needed. To accelerate such efforts, the development of JS016, a neutralizing monoclonal antibody directed against the SARS-CoV-2 spike protein, was expedited from a typical 12- to 18-month period to a 4-month period. During this process, transient Chinese hamster ovary cell lines are used to support preclinical, investigational new drug-enabling toxicology research, and early Chemistry, Manufacturing and Controls development; mini-pool materials to supply Phase 1 clinical trials; and a single-clone working cell bank for late-stage and pivotal clinical trials were successively adopted. Moreover, key process performance and product quality investigations using a series of orthogonal and state-of-the-art techniques were conducted to demonstrate the comparability of products manufactured using these three processes, and the results indicated that, despite observed variations in process performance, the primary and high-order structures, purity and impurity profiles, biological and immunological functions, and degradation behaviors under stress conditions were largely comparable. The study suggests that, in particular situations, this strategy can be adopted to accelerate the development of therapeutic biopharmaceuticals and their access to patients.

Introduction

The spread of the severe acute respiratory syndrome coronavirus 2 (SARS-CoV-2), a novel virus currently causing one of the most devastating pandemics of the modern era,[1] occurred rapidly across the world, with more than 190 million confirmed cases and 4.1 million deaths confirmed globally by the end of February 2021, according to the World Health Organization. The coronavirus disease 2019 (COVID-19) pandemic has propelled global collaborative efforts, with scientists racing to develop effective medicines and therapeutics to curb the spread of the virus and treat infected patients. Among the treatment options for COVID-19 that have been explored, antiviral small-molecule agents,[2] immunomodulators,[3] protease inhibitors,[4] convalescent plasma,[5] have attained mixed results in the treatment of infected patients in varying stages of their disease process. COVID-19–neutralizing antibodies derived from the convalescent plasma of COVID-19 survivors or other sources have been increasingly adopted, with emerging evidence as one of the most promising treatment options, especially for patients with mild-to-severe infections and as a preventive measure for immuno-vulnerable groups such as young children and adults older than 65 years of age.[6–8] According to the COVID-19 biologics tracking website,[9]

there are more than 100 monoclonal antibody drugs under development and 23 candidates advancing through clinical stages. Three monoclonal antibody treatments, namely casirivimab/imdevimab (REGN-COV2; Regeneron),[10] bamlanivimab (LY-CoV555, LY3819253)/etesevimab (JS016) (Eli Lilly and partners' AbCellera/NIAID and Junshi Biosciences),[11] and sotrovimab (VIR-7831, GSK4182136; VIR Biotechnology, GlaxoSmithKline), were authorized for emergency use for the treatment of mild-to-moderate COVID-19 in adult and pediatric patients by the United States Food and Drug Administration and the European Medicines Agency. Meanwhile, results from a recent Phase 3 clinical trial (BLAZE-1) of the bamlanivimab/etesevimab combination treatment indicated a remarkable 87% reduction in the risk of COVID-19-related hospitalizations and deaths in a high-risk population compared with a placebo group.

JS016 (etesevimab) is a human immunoglobulin G1 (IgG1) antibody produced from a Chinese hamster ovary (CHO) cell line, with engineered Fc chains to diminish potential FcγRs-associated effector functions.[7] JS016 neutralizes SARS-CoV-2 by high-affinity binding to the S1 domain of the receptor-binding domain (RBD) of the spike protein, preventing the

virus' interaction with the human angiotensin-converting enzyme 2 (ACE2), which is the main mechanism facilitating the entry of SARS-CoV-2 into host cells. Urged by the urgent need for effective COVID-19 treatments, the development path of JS016 has exploited an expedited strategy to shorten the timeline of the development of the therapeutic to achieving an investigational new drug (IND) status from a typical length of 12–18 months of industry development timeframe to only a 6-month period.[12,13] Just recently, Zhang et al. applied the Chemistry, Manufacturing and Controls (CMC) strategies of pool materials for toxicology study by reshaping cell line development within 6 months.[14] We further expedited the development path of JS016, using transient cell lines materials to support IND-enabling toxicology study to shorten the timeline to only a 4-month period. The strategy uses the following: (1) a 200-L bioreactor production scale with transient CHO cell lines to support preclinical, IND-enabling toxicology research, and early CMC development; (2) utilization of mini-pool materials to supply Phase 1 clinical trials; and (3) supply ensuing late-stage and pivotal trial materials with production from established single-clone working cell bank (WCB). The in-house biologics manufacturing process and analytical platform survive the pressure test brought on by the unconventionally fast-tracked timeline and help to yield robust process performance and comparable product quality. Here, we focus on assessing the comparability of key process performances and product quality across the 200-L transient cell materials, the 2,000-L mini-pool materials and the 2,000-L single-clone WCB materials.

Table 1. Comparability testing categories and analytical methods of JS016.

Category	Analytical Technique
Process comparison	Process controls
Primary structure	Intact molecular mass with and without deglycosylation
	Reduced molecular mass with and without deglycosylation
	Protein primary sequence by reduced peptide mapping
	Disulfide bond structure by reduced and non-reduced peptides
	N-glycan profiling by HILIC–HPLC
	Free thiol content by Ellman's assay
	Isoelectric point by iCIEF
Higher-order structure	Secondary structure by MMS
	Tertiary structure by near-UV CD
	Thermal stability by DSC
Product-related substances and impurities	Size variants by SEC HPLC, rCE-SDS, and nrCE-SDS
	Charge variants by CEX HPLC
Process-related impurities	Residual protein A by ELISA
	Residual host cell DNA (HCD) by qPCR
	Residual host cell protein (HCP) by ELISA
Biological activity	RBD-S1 binding assay by ELISA
	RBD-S1 blocking assay by ELISA
	Neutralization assay by pseudovirus-dependent cell-based bioassay
Biological functions	RBD affinity by SPR
	FcRn binding by BLI
	FcγRIa binding by BLI
	FcγRIIa(R167) binding by BLI
	FcγRIIa (H167) binding by BLI
	FcγRIIb binding by BLI
	FcγRIIIa (V176) binding by BLI
	FcγRIIIa (F176) binding by BLI
	FcγRIIIb binding by BLI
	C1q binding by BLI
Forced degradation	Thermal stability at 50°C assessed by purity and potency
	Light stability assessed by purity and potency

Results

An extensive set of analytical techniques and assays were used to assess the physicochemical and biological properties and other quality profiles of JS016 materials manufactured using three different processes. The full method set and respective quality attributes in focus are shown in (Table 1) and the complete dataset is presented in Supplemental Tables. Where applicable, orthogonal methods were used to extensively interrogate critical product attributes.[15] A few changes to the strength and formulation were implemented throughout the development of the neutralizing antibody, JS016. Protein concentrations were raised from 20 to 40 mg/mL and finally to 100 mg/mL,

spanning across the preclinical to clinical stages. The formulation components were also switched from a mannitol to sucrose-based formulation to enhance protein stability.

The analytical comparability studies included comprehensive assessments of molecular attributes, such as process performances, primary structures, higher-order structures, product-related substances and impurities, process-related impurities, biological activity and functions, and accelerated stability. This provided data for a comparative and quantitative products attribute profiles database, enabling statistically meaningful comparisons per regulatory agency guidance and providing concrete supporting evidence for the analytical comparability assessment.

Table 2. Source of lots for comparison.

| Process Instance	Cell Line	Bioreactor Size	Number of Runs	Lot IDs	Formulation Buffer
Proc-A	Transient	200 L	n = 3 lots	Lot A001 Lot A002 Lot A003	20 mM of L-histidine/L-histidine hydrochloride (pH: 6.0), 247 mM of mannitol, 0.02% polysorbate 80
Proc-B	Stable Pool	2,000 L	n = 3 lots	Lot B001 Lot B002 Lot B003	20 mM of L-histidine/L-histidine hydrochloride (pH: 6.0), 247 mM of mannitol, 0.02% polysorbate 80
Proc-C	Monoclonal	2,000 L	n = 3 lots	Lot C001 Lot C002 Lot C003	20 mM of L-histidine/L-histidine hydrochloride (pH: 6.0), 235 mM of sucrose, 0.02% polysorbate 80
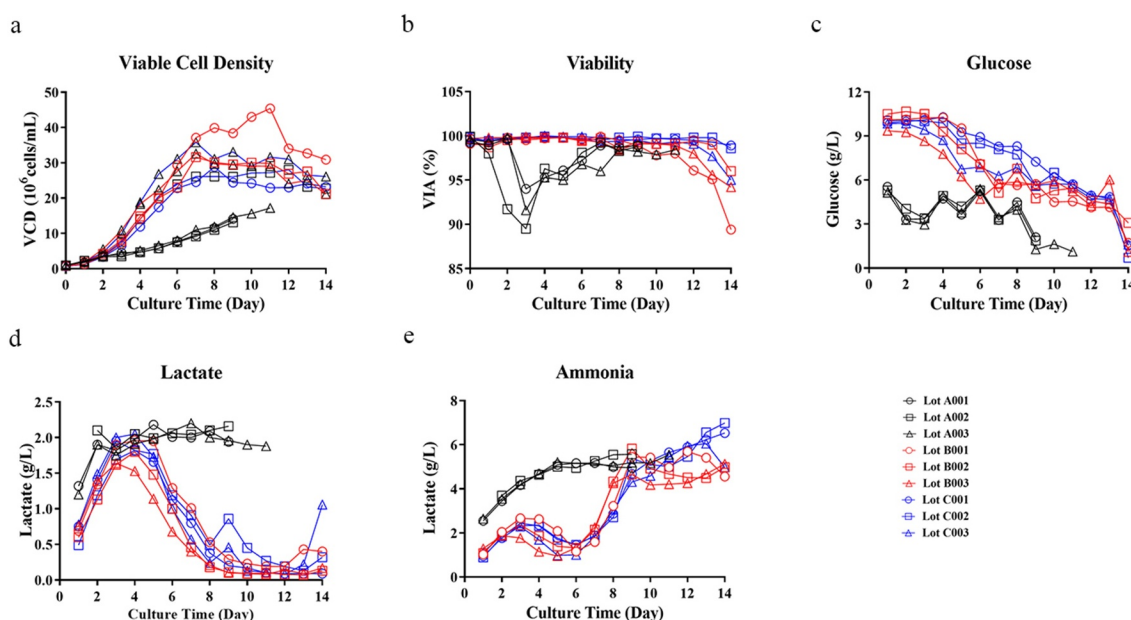
Figure 1. In-process monitoring results of the production N-stage bioreactor of Proc-A, Proc-B and Proc-C. (a) Viable cell density, (b) cell viability, (c) glucose metabolism parameter, (d) lactate metabolism parameter, (e) ammonia metabolism parameter.

Process comparison

We present here a comparison (Table 2) of the performance of JS016 cell cultures for three different process instances – specifically, processes A, B and C (referred to as Proc-A, Proc-B and Proc-C, respectively), which sequentially evolved during the development lifecycle for different preclinical and clinical supply purposes. In-process testing and in-process controls of the production bioreactor are presented here for review to assess the performance impact and factors affecting performance.

Bioprocess reactor profiles can be affected by host cell line genetics and metabolomics, particularly transfection (i.e., clonality and stability), culture media formulation and feed strategies; and even the configuration of reactor controls (i.e., batch sequence and controller tuning). Figure 1 shows in-process testing/monitoring results of the N-stage bioreactor production. Note that the figure presents important cell growth (viable cell density, cell viability) and cell metabolism (glucose, lactate, ammonia) parameters.

All three process instances showed good batch-to-batch consistency, but the Proc-A group results were observed to be different from those of the Proc-B or Proc-C group. Specifically, Proc-A used a transient transfection process, while Proc-B and Proc-C adopted stably transfected cells for production. Lab-scale transient transfection/expression is often used in research and development to deliver milligram-quantity levels. In our case, we can assume that the transient transfection cell pools and stable transfection cell pools were what led to the variable process performance results (i.e., Proc-A vs. Proc-B and Proc-C).

Proc-B used a stable pool cell bank, while Proc-C used a single-cell clone cell bank. Proc-C monoclonality was obtained via single-cell isolation from the Proc-B stable pool cell bank.

By comparing Proc-B and Proc-C, we observed no significant impact on the upstream in-process cell growth (viable cell density, cell viability) or cell metabolism (glucose, lactate, ammonia) parameters (i.e., Proc-B vs. Proc-C).

Primary structure

To assess whether the three processes resulted in comparable primary structures of JS016, advanced technologies with high sensitivity and mass accuracy were used, including ultra-high performance liquid-chromatography (UPLC)-mass spectrometry (MS) and liquid chromatography (LC)-MS/MS. Two complementary enzymatic digestions using trypsin or chymotrypsin were used to ensure 100% amino acid sequence coverage. N-terminal and C-terminal sequence confirmations were also ensured, and molecular masses of intact and reduced (i.e., with and without N-linked glycans) were compared. Disulfide linkage analysis using non-reduced peptide mapping by Lys-C and trypsin with comparison to the reduced peptide mapping was completed to demonstrate identical disulfide bond linkages for the tested lots. Finally, the N-glycosylation site was confirmed by LC-MS/MS, and the free thiol content was determined using Ellman's assay.

The measured masses for all samples had a close correlation with the theoretical masses computed according to the primary amino acid sequences, including the conversion of Asn299 to Asp299 as a result of the removal of the N-glycans by PNGase F and the truncation of the C-terminal lysine on the heavy chain (HC). As shown in Supplemental Table S1, the intact molecular masses of samples with glycosylation ranged from 147,814 to 147,817 Da, and the masses with deglycosylation ranged from 144,924 to 144,927 Da; all existed within the 10-ppm mass error of the theoretical mass of the JS016 molecule.

The molecular masses of reduced and deglycosylated drug substances presented additional evidence that the HC and light chain (LC) polypeptide compositions were comparable among the different processes. The reduced HC masses totaled 50,306 Daltons for HC with major glycoform G0F, while the reduced LC masses ranged from 23,604 to 23,605 Daltons for the three process products. Additionally, the reduced HC masses were all 48,861 Daltons for samples with deglycosylation, and no change in the reduced LC masses was observed as expected.

The reduced LC-MS/MS peptide maps of all samples exhibited comparable peak profiles, with closely matched peak intensities and retention times (Figure 2); this further confirmed that the JS016 products from the three processes possess the same primary structure. Meanwhile, the combined trypsin and chymotrypsin peptide mapping analysis collectively covered 100% of the amino acid sequence of the theoretical JS016 protein sequence.

The major post-translational modification (PTM) sites and comparable modification profiles are described below. The conserved Asn299 sites were the only N-glycosylation sites, with the G0F, G1F, and G2F family as the dominant glycoforms accounting for more than 92% of total N-glycans, together with nine other minor glycan species. Other major PTMs were as follows: cyclization of the Glu residue of N-terminal HC to form a pyroglutamate moiety (pE) was presented in the range of 2.2–z4.5%; C-terminal Lys truncation of HC ranged from 97.4% to 99.5%; Met 101 and Met 254 were the main sites vulnerable to oxidation with levels of less than 2% in all process materials; and, lastly, deamidation of Asn residues were observed at low levels (<1.6%) for all three processes. The deamidation levels, especially at Asn386 and Asn391 in the PENNY loop, were higher in Proc-B and Proc-C samples, which could be caused by the longer fermentation culture time. All peptide modifications, together with their respective sites and levels, are presented in Supplemental Table S2.

To determine the disulfide bond connectivity, non-reduced peptide mapping was conducted by LC-MS/MS after Lys-C/ trypsin enzymatic digestion. By comparing the reduced and non-reduced peptide maps for unique disulfide bond–associated peaks and signature MS^2 fragment ions, the unambiguous identification of disulfide bond mapping (Supplemental Table S3) showed that all samples contained a total of 32 cysteine residues, forming 4 inter-chain and 12 intra-chain disulfide bond pairs, respectively. Moreover, the linkage profiles were conformed to the theoretical disulfide bond structure of a typical IgG1 antibody. In addition, the free thiol content of all samples was below 0.3% mol/mol (free thiols/per intact IgG) as per the Measure-IT™ thiol assay, as shown in Table 3. These findings demonstrated that all JS016 samples contain the same disulfide linkages, and no mismatched disulfide bonds were observed. Residual free thiols were present in trace amounts in all three processes materials.

The overlay N-glycan maps for JS016 are shown in Figure 3. The results demonstrate that all samples had comparable profiles, with a total of 12 glycan forms above 0.2% and all major glycans are present in three processed materials. Minor differences in Man5 and G1F content were observed. As shown in Table 3, the most five abundant glycans (G0F-GN, G0, G0F, G1F and G1F-GN) and four glycan groups (high mannose, afucosylation, galactosylation and sialic acid) were evaluated as part of the comparability assessment based on their potential to affect pharmacokinetics (PK) or biological functions, including binding to crystallizable fragment (Fc) receptors. Minor differences in high mannose and galactosylation content were observed between the three processes. The high mannose species in Proc-A samples totaled about 0.4% higher than those of the samples from Proc-B or Proc-C. It has been reported that high mannose species may support a faster clearance rate than biantennary complex counterparts. However, given the overall low percentage of the high mannose species in JS016, this residual glycan difference would have a negligible clinical impact. Slightly higher levels of galactosylation was observed in the stable CHO compared to the transient process, but the minor difference has no effect on C1q binding activity (Table 4) since JS016 is engineered with Leu234Ala/
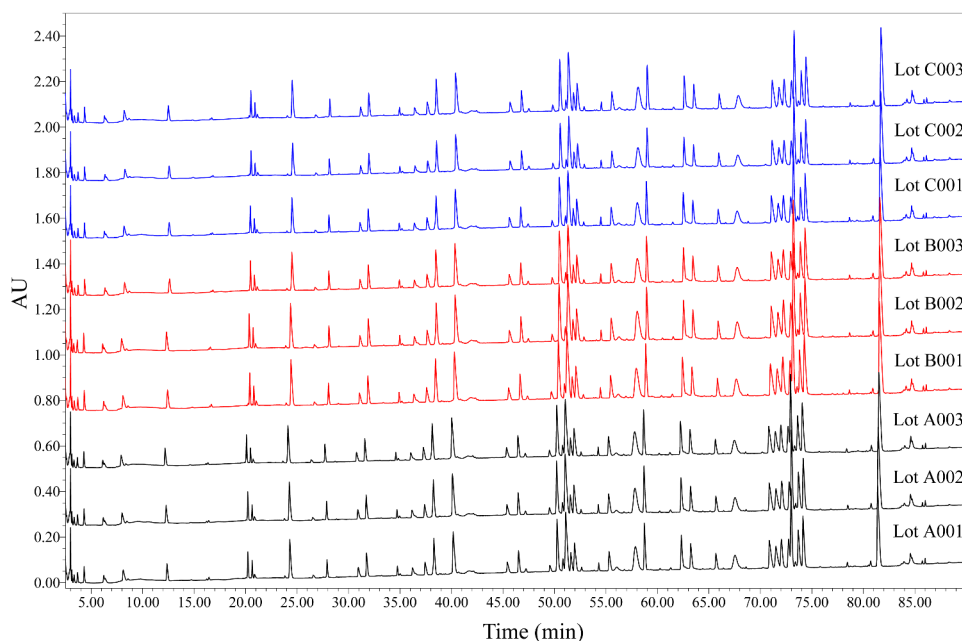

Figure 2. Peptide maps of trypsin digested of Proc-A, Proc-B and Proc-C drug substances.

Table 3. The free thiol content, N-glycan results, similarity values of secondary structure, Tm values, product-related substances and impurities, process-related substances and impurities of Proc-A, Proc-B and Proc-C drug substances.

Attributes		Proc-A			Proc-B			Proc-C		
		Lot A001	Lot A002	Lot A003	Lot B001	Lot B002	Lot B003	Lot C001	Lot C002	Lot C003
Free thiol content (mol SH/mol IgG)		0.10	0.05	0.26	0.21	0.09	0.13	0.07	0.13	0.19
N-glycan	G0F-GN (%)	1.14	1.23	1.15	1.10	2.60	2.45	1.94	1.15	0.65
	G0 (%)	1.65	1.64	1.71	1.65	1.91	1.50	1.90	2.02	1.76
	G0F (%)	91.11	91.26	91.18	88.02	91.25	91.64	90.63	88.05	87.26
	G1F (%)	1.45	1.34	2.00	5.92	0.85	0.98	2.34	5.57	6.92
	G1F-GN (%)	1.07	1.04	0.99	0.33	0.77	0.76	0.67	0.32	0.33
	High mannose (%)	0.97	0.93	1.21	0.52	0.64	0.59	0.62	0.62	0.52
	Afucosylation (%)	1.75	1.74	1.81	1.74	2.04	1.62	1.99	2.13	1.91
	Galactosylation (%)	2.80	2.75	2.36	6.86	1.82	1.93	3.33	6.47	8.03
	Sialic acid (%)	0.11	0.14	0.09	0.10	ND	0.04	0.06	0.06	0.09
Similarity values of secondary structure (%)		98.93 ± 0.08	98.70 ± 0.31	98.88 ± 0.28	99.76 ± 0.06	99.64 ± 0.04	99.50 ± 0.05	99.03 ± 0.04	99.19 ± 0.10	99.02 ± 0.21
T_m values	T_m1 (°C)	71.17	71.19	71.20	71.22	71.23	71.24	71.42	71.47	71.51
	T_m2 (°C)	79.08	79.07	79.05	79.01	79.02	79.00	79.24	79.24	79.24
	T_m3 (°C)	85.32	85.32	85.32	85.33	85.33	85.33	85.75	85.76	85.76
SEC	HMW (%)	0.3	0.3	0.2	0.6	0.5	0.5	0.3	0.3	0.2
	Monomer (%)	99.7	99.7	99.8	99.4	99.5	99.5	99.7	99.6	99.7
rCE-SDS	HC+LC (%)	98.9	98.8	98.5	98.6	98.7	98.4	98.7	98.6	98.6
	NGHC (%)	0.4	0.4	0.5	0.3	0.2	0.3	0.3	0.3	0.3
nrCE-SDS	Main peak (%)	98.0	98.0	98.2	97.7	97.2	97.2	97.1	97.4	97.6
	Impurity (%)	2.0	2.0	1.8	2.3	2.8	2.8	2.9	2.6	2.4
CEX	Acidic peaks (%)	11.6	10.6	10.6	16.5	13.3	14.8	11.8	11.8	12.8
	Main peak (%)	86.1	87.2	87.3	81.8	85.1	83.7	86.4	86.4	85.5
	Basic peaks (%)	2.2	2.2	2.0	1.7	1.7	1.7	1.8	1.8	1.8
Residual protein A (ppm)		< 0.3	< 0.3	1.6	< 0.3	< 0.3	< 0.3	< 0.3	< 0.3	< 0.4
Residual host cell DNA (pg/mg)		< 1.1	< 1.0	< 1.1	<1.0	< 0.5	< 0.5	< 0.5	< 0.5	< 0.5
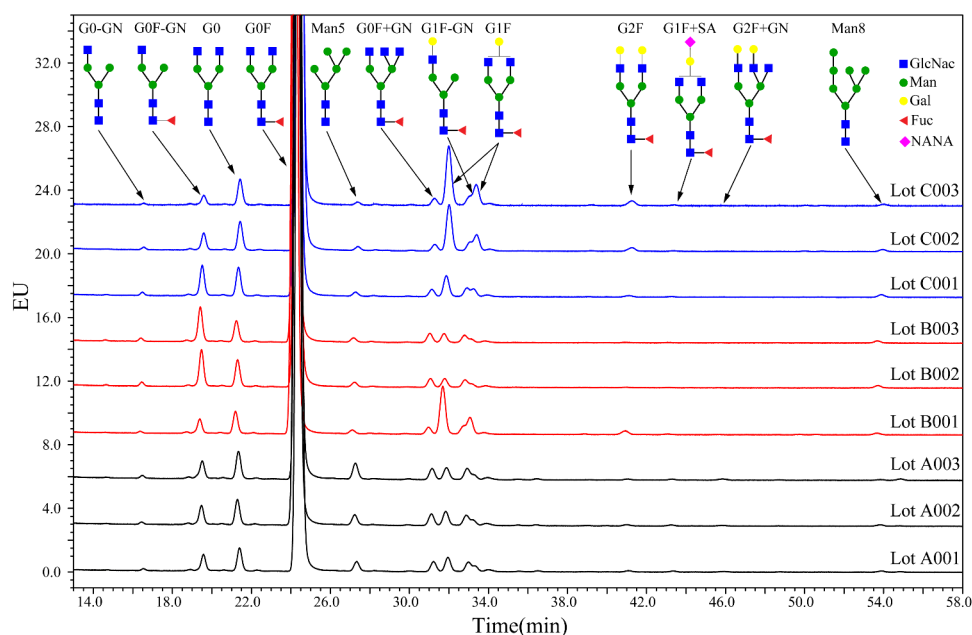
Figure 3. N-glycan maps of Proc-A, Proc-B and Proc-C drug substances.

Leu235Ala (LALA) mutations to diminish FcγRs-mediated antibody-dependent cell-mediated cytotoxicity (ADCC), antibody-dependent cellular phagocytosis (ADCP) and complement-dependent cytotoxicity (CDC) activities.[16]

Imaged capillary isoelectric focusing (iCIEF) was used to determine the apparent isoelectric point (pI) of JS016. The iCIEF profiles of JS016 are comparable and the pI value of the main isoform was determined to be 8.8 for all tested lots, as shown in Supplemental Figure S1.

Higher-order structures

The higher-order structures of JS016 lots were characterized using an array of biophysical techniques. Results of the secondary structure analysis by microfluidic modulation spectroscopy (MMS),[17] tertiary structure analysis by ultraviolet circular dichroism (UV CD), and thermal stability analysis by differential scanning calorimetry (DSC) are shown in Figure 4 (a)–(c), respectively.

Table 4. Summary of biological and functional activity for JS016 drug substances.

Attributes		Proc-A			Proc-B			Proc-C			Wild-type Control
		Lot A001	Lot A002	Lot A003	Lot B001	Lot B002	Lot B003	Lot C001	Lot C002	Lot C003	JS016-WT
Fab-mediated functions	RBD-S1 blocking (%)	106	95	88	102	102	111	101	99	91	NT
	RBD-S1 binding (%) (ELISA method)	94	84	102	94	93	89	101	98	93	NT
	Neutralization potency (%)	105	90	89	96	79	90	71	111	102	NT
	RBD-S1 binding affinity (M) (BIL method)	2.4E-08	2.7E-08	2.9E-08	2.9E-08	2.8E-08	2.6E-08	3.0E-08	2.8E-08	2.8E-08	2.7E-08
Fc-mediated functions (M)	FcRn binding	7.6E-08	7.4E-08	8.0E-08	6.8E-08	5.3E-08	4.5E-08	6.0E-08	3.7E-08	6.2E-08	6.8E-08
	FcγRI binding	9.1E-07	6.5E-07	6.8E-07	7.9E-07	7.6E-07	7.5E-07	9.7E-07	8.2E-07	8.6E-07	5.7E-09
	FcγRIIa (R167) binding	2.5E-05	3.4E-05	3.9E-05	5.6E-05	3.1E-05	2.7E-05	3.6E-05	3.7E-05	4.5E-05	1.6E-06
	FcγRIIa (H167) binding	3.2E-05	6.3E-05	6.2E-05	8.1E-05	4.4E-05	3.2E-05	4.3E-05	4.5E-05	5.9E-05	1.7E-06
	FcγRIIb binding	6.4E-05	6.2E-05	6.3E-05	5.4E-05	5.4E-05	5.5E-05	7.2E-05	5.9E-05	7.2E-05	2.4E-06
	FcγRIIIa (V176) binding	1.1E-05	1.3E-05	1.1E-05	1.3E-05	1.3E-05	1.1E-05	1.6E-05	1.7E-05	1.6E-05	6.1E-07
	FcγRIIIa (F176) binding	2.2E-05	2.6E-05	2.3E-05	1.9E-05	2.2E-05	1.8E-05	1.5E-05	1.9E-05	1.7E-05	2.0E-06
	FcγRIIIb binding	WB	WB	WB	WB	WB	WB	WB	WB	WB	2.8E-06
	C1q binding	NB	NB	NB	NB	NB	NB	NB	NB	NB	2.12E-09
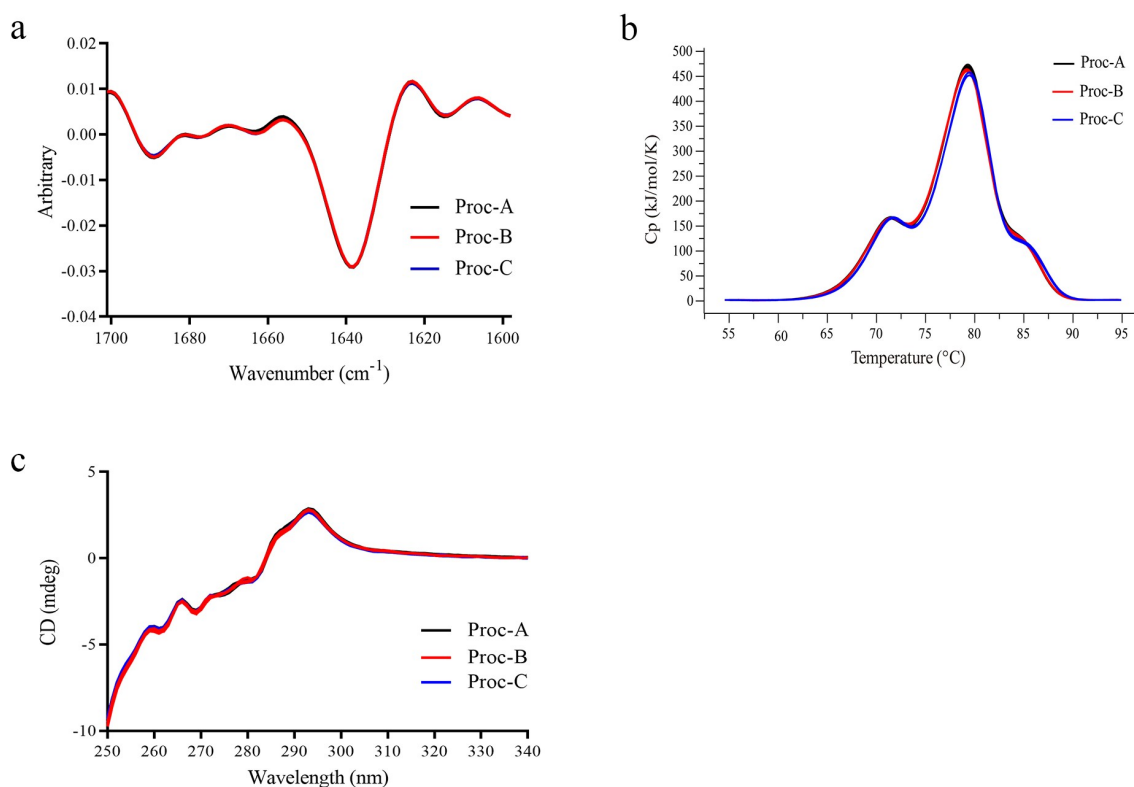
Figure 4. Higher order structure. (a) MMS spectra, (b) Near-UV CD spectra, (c) DSC spectra.

The MMS profiles were visually comparable for JS016 samples (Figure 4(a)). The spectra exhibited strong β-sheet band signal patterns at around 1,639 cm^{-1} and 1,689 cm^{-1}, as well as a β-turn band at around 1,670 cm^{-1}, indicating the abundance of the antiparallel β-sheet structure typically observed in antibodies. Using the reference spectrum of the reference materials as a benchmark, the spectral similarity value of all samples was greater than 98% (Table 3), indicating comparable secondary protein structures among the study subjects.

The DSC profiles of all JS016 samples were visually comparable and superimposable (Figure 4(b)). The DSC thermograms boasted three endothermic thermal transitions corresponding to the unfolding of the constant CH2 domain, the antigen-binding fragment (Fab) and the constant CH3 domain, respectively. Each transition was characterized by a unique DSC thermal melting temperature (Tm1, Tm2 and Tm3).[18] The Tm1, Tm2 and Tm3 values of three separated processes were closely matched as is summarized in Table 3. The thermal stabilities of the three processing materials were highly comparable.

The near-UV CD profiles were visually comparable across all the samples (Figure 4(c)). The near-UV spectra contain signals from tryptophan, tyrosine and phenylalanine, which are superimposed on the broad disulfide bond signal from 250 to 280 nm, indicating the presence of a native tertiary structure and suggesting that the disulfide bonds and aromatic amino acids reside in a highly similar microenvironment owing to proper folding of proteins.

Product-related substances and impurities

Several combined approaches to evaluate size and charge variants were used to assess product-related substances and impurities.

The size variants of samples were determined by size-exclusion high-performance liquid chromatography (SEC HPLC), reduced capillary electrophoresis–sodium dodecyl sulfate (rCE-SDS) and non-reduced (nr) CE-SDS. Aggregates were assessed by SEC HPLC under native conditions, whereas CE-SDS was used for the separation of denatured size variants of proteins under reduced or non-reduced conditions. All lots attained greater than 99% monomeric antibody (Table 3) with comparable retention times in SEC HPLC. Aggregate levels of the study materials were consistently below 0.7% and slightly higher aggregate levels (~0.3%) were observed in Proc-B samples as compared to those in the Proc-A or Proc-C materials (Figure 5(a) and Table 3). Judging by the shift of the retention time, there seems to be less larger aggregates in Process C materials. Both reduced and non-reduced CE-SDS profiles and patterns are highly consistent among the tested materials (Figures 5(b,c) and Table 3), except for some minor differences. For instance, ~0.8% lower intensity for the post-HC impurity peaks from the Proc-A samples was observed in the reduced CE-SDS. This post-HC impurity pattern was determined using a reduced mass and peptide mapping method as a thioether bond cross-linked between HC and LC (Supplemental Figures S2 and S3 and Supplemental Table S4). Meanwhile, Proc-B and Proc-C materials revealed about ~0.7% higher levels of fragments (pre-main peak) in nrCE-SDS as compared to Proc-A materials, and this fragment pattern was attributed to the heavy-heavy-light chain (HHL) species.

Charge variants were evaluated by CEX HPLC. All three sets of samples had comparable charge variant profiles with a main peak ratio in the range of 81.3–87.3%. Slightly higher levels (~3%) of acidic variants were reported for the Proc-B samples as shown in Figure 5(d) and Table 3. Further characterization by peptide mapping showed that highly similar PTM sites and propensities were present with all samples except the deamidation levels. The difference of chromatograms in Figure 5(d) for Proc-B and Proc-C acidic groups compared with Proc-A could be explained by higher deamidation levels at the Asn398 and Asn391 in the PENNY loop. Such minor charge variant differences would be expected to have a negligible impact on the biological activities of JS016.

Process-related impurities

Process-related impurities, such as residual protein A, host cell protein (HCP) and host cell DNA (HCD), are under tight scrutiny and control owing to their potential adverse effects on patient safety. Residual protein A and HCPs were assessed by ELISA-based methods, and residual HCD was determined
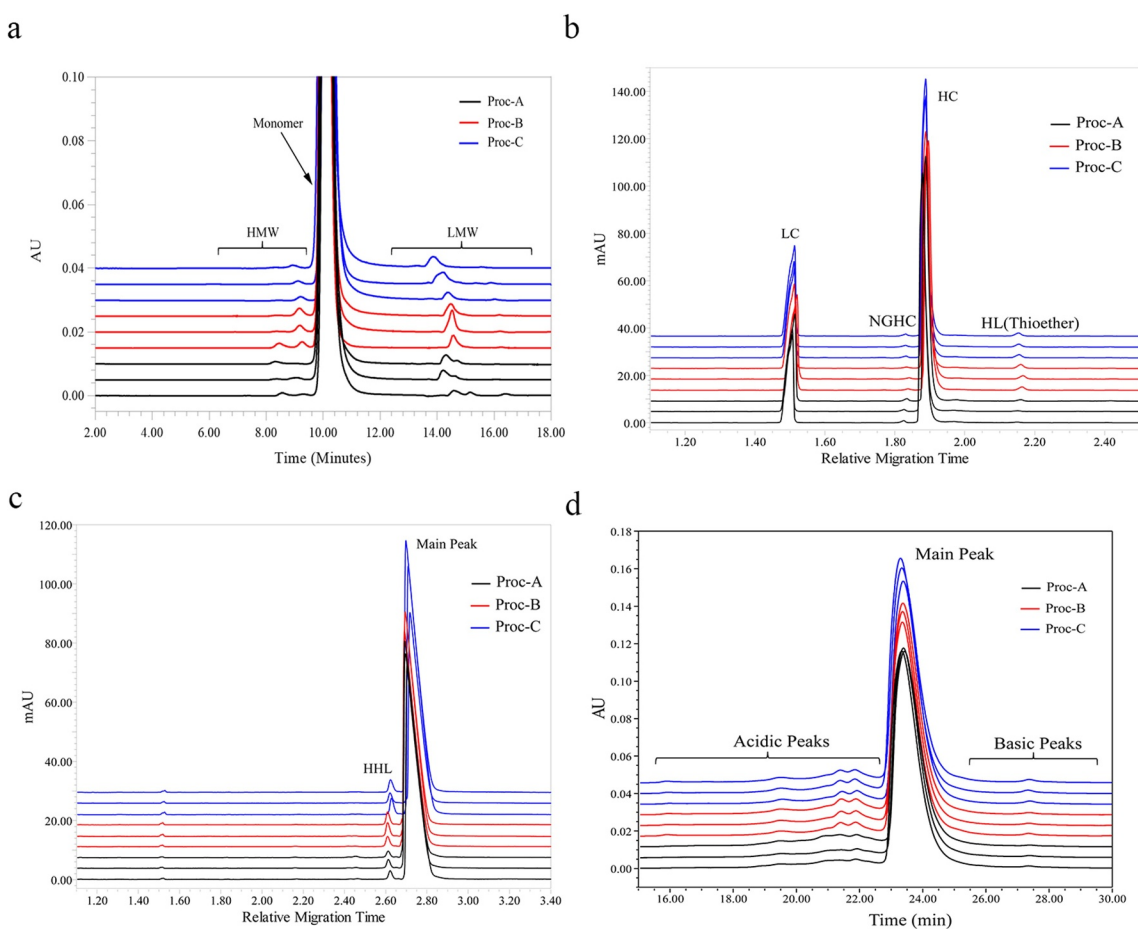

Figure 5. Comparison of the size and charge variants by SEC-HPLC (a), rCE-SDS (b), nrCE-SDS (c), and CEX-HPLC (d) of Proc-A, Proc-B and Proc-C drug substances.

by quantitative polymerase chain reaction (qPCR).[19] As shown in Table 3, these process-related impurities were present in substantially low levels or below the quantitation limit in all drug substances.

Biological and functional activity

The comparability of biological activity of JS016 samples was evaluated by antigen-specific and Fc-effector-specific biological functions as listed in Table 1. JS016 is engineered with LALA mutations to diminish FcγRs-mediated ADCC, ADCP and CDC activities in the virus-defending monoclonal antibody,[16] and the binding affinity of JS016 to FcγRI and FcγRIIIa(V176) is substantially suppressed with an approximately two-magnitude reduction relative to the wild-type control. A moderate modulation of binding affinity is observed for other FcγRs. It is worth mentioning that materials from all three processes yielded consistent effector receptor-binding affinities across the studied Fcγ receptors (FcγRI, FcγRIIa (R167), FcγRIIa (H167), FcγRIIb, FcγRIIIa (F176), FcγRIIIa (V176), FcγRIIIb and complement C1q binding. The results of biological assays are summarized in Table 3.

The neonatal Fc receptor (FcRn) binds to the Fc region of IgG and maintains IgG homeostasis in the circulation. All JS016 samples had comparable FcRn binding affinities (Table 4). Moreover, the affinity to FcRn was unaffected by LALA mutations and all lots yielded similar binding affinities to that of the wild-type control. Overall, the biological activity results supported the comparability of the three processed drug substances.

JS016 binds to the RBD-S1 domain of the spike protein of SARS-CoV-2 with high affinity, which plays a critical role in neutralizing this virus in clinical settings. The comparability assessment included binding and blocking potency as measured by ELISA assay, RBD binding affinity determined by SPR, and neutralization assay. All the biological activity results, including binding, blocking, neutralization potency and antigen affinity, were demonstrated to be comparable as shown in Table 4 and Figure 6.

NT: not tested; WB: weak binding; NB: no binding.

Forced degradation stability

During the analytical comparability assessment, forced degradation studies were conducted to elucidate product-degradation pathways and rates among the different process materials. One drug product lot each from Proc-A, Proc-B and Proc-C was subject to a comparative forced degradation investigation and alterations in the stability-indicating attributes were evaluated with by SEC HPLC, nrCE-SDS, rCE-SDS, CEX HPLC,and potency assays.

JS016 materials from the three manufacturing processes exhibited similar degradation trends and profiles under both thermal and light stress (Figures 7 and 8). Low molecular weight (LMW) levels slightly increased to ~1% after incubation at 40°C for 20 days for all three samples, and the main peaks decayed at a similar, slow rate. Conversely, high molecular weight (HMW) levels remained largely unchanged throughout the course of the thermal stress. As for the CEX results, all three JS016 lots showed a similar trend of an increasing acidic peak percentage at a rate of 0.6% per day with concurrent reduction
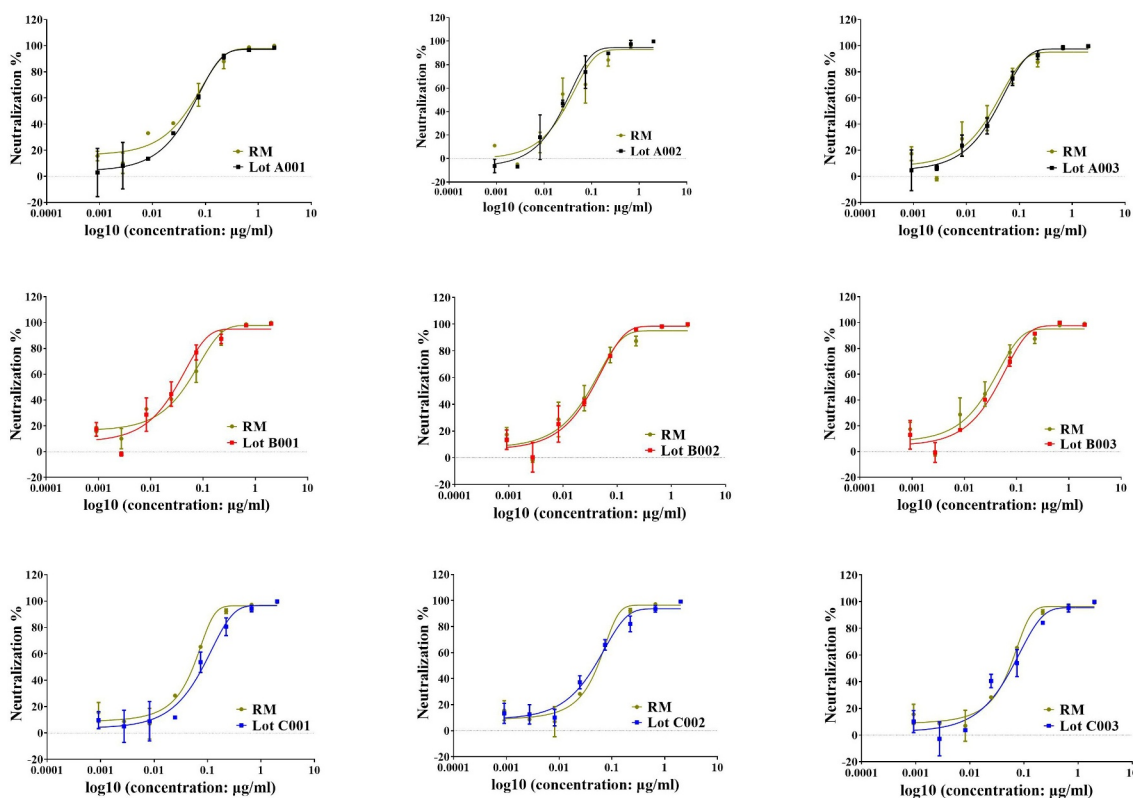

Figure 6. Virus neutralization potency of Proc-A, Proc-B and Proc-C drug substances.
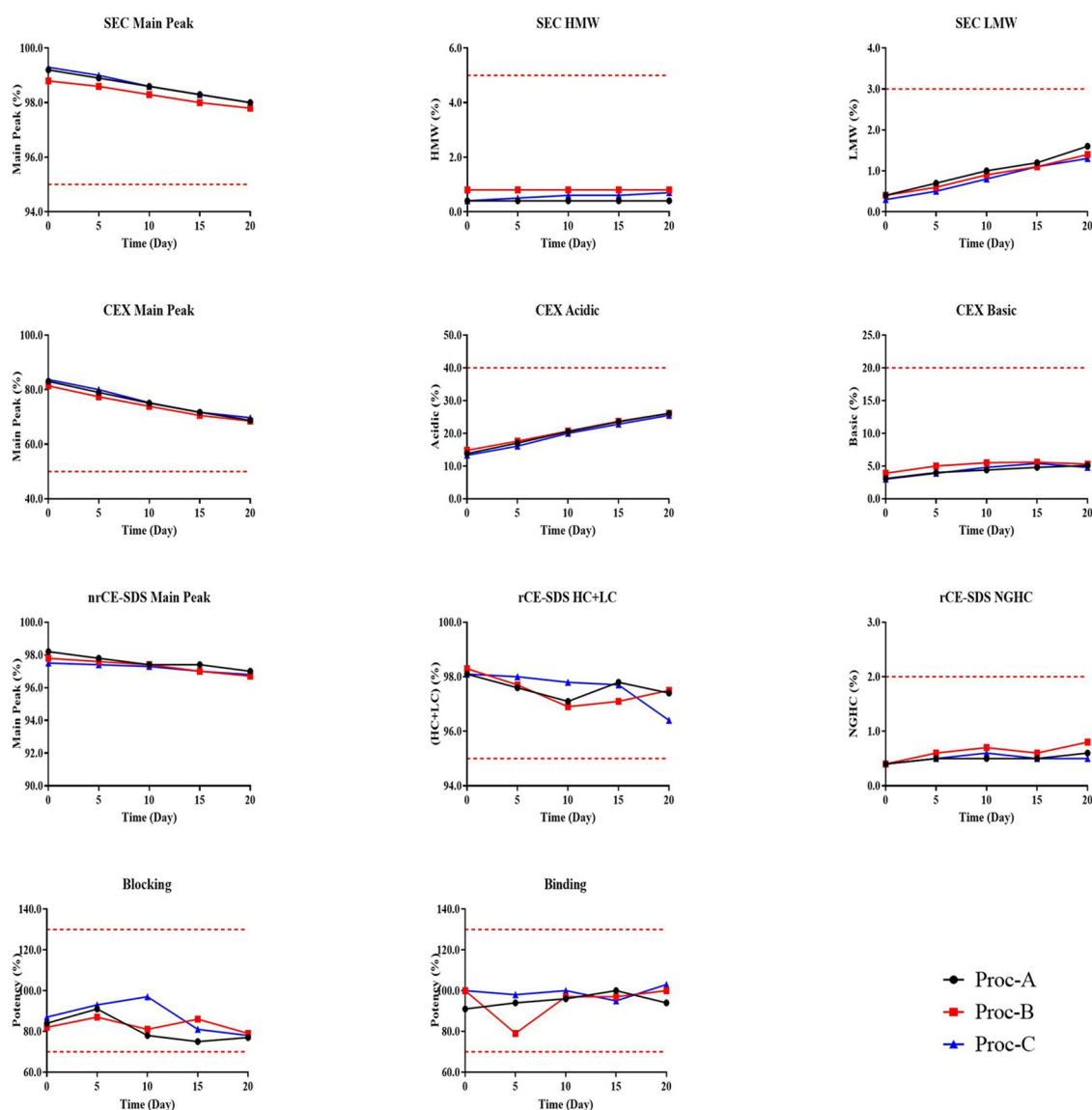
Figure 7. Time-course SEC, CEX, nrCE-SDS, rCE-SDS and potency results of Proc-A, Proc-B and Proc-C products under high temperature (40°C, RH 60%).

of the main peak at a rate of 0.6–0.7% per day. However, basic peak levels were less affected under thermal stress, and minor changes in nrCE-SDS and rCE-SDS results occurred for the thermal stress samples, which were confined in a ~ 1.5% change window. All biological assays showed no thermally induced loss of the biological activities of JS016.

Light illumination induces different degradation profiles in contrast to thermal stress. JS016 again showed excellent resistance in terms of size variant stability. The main peak of SEC results decayed by less than 3% in a 20-day span. The loss of the main peak was contributed to by both the rise in HMW and LMW species. The nrCE-SDS and rCE-SDS results conformed to the same trends as those observed via SEC HPLC. A much faster decay rate of nearly 30% in the CEX main peak during the study period was observed with light treatment. Both acidic and basic peaks were elevated significantly at similar paces for all three processed materials. The biological activities of light-stressed JS016 showed a declining trend and edges above the preset lower-quality specification (70%) of both the relative

blocking and binding activities; one exception was the last time point for the Proc-A material, which fell slightly below the 70% mark. Overall, extended light exposure seems to have a more pronounced impact on the physiochemical properties and biological activities of JS016 materials. Therefore, it is recommended to store the JS016 drug product with protection from light. It is noteworthy that the light-protected controls within the same chamber (Supplemental Figure S4) experienced little changes relative to the monitored attributes regardless of the stress conditions. In conclusion, comparable degradation profiles and pathways of three process products considering thermal and light stress conditions were demonstrated.

Discussion

A head-to-head comparability study was conducted in a 3:3:3 design, and the results showed that the samples of the three different processes were comparable to one another. The
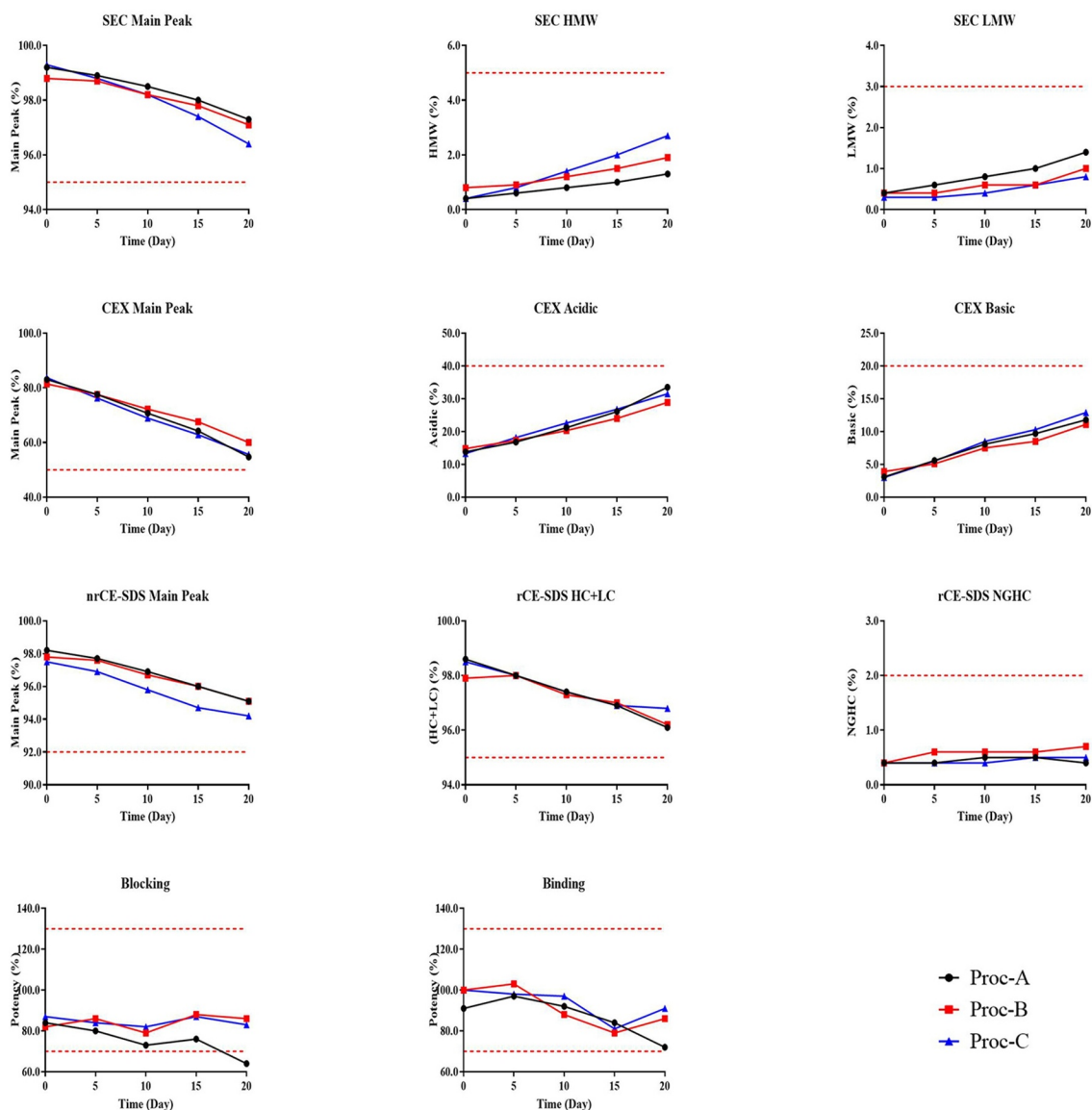
Figure 8. Time-course SEC, CEX, nrCE-SDS, rCE-SDS and potency results of Proc-A, Proc-B and Proc-C products under light exposure (4500 ± 500 lux).

comparability research included the following five categories: process performance, structure characterization, purity and impurity, biological activity and forced degradation stability. Although minor differences were observed in the comparability study results, they do not affect the comparability conclusions. During the process performance section of the investigation, Proc-A process characteristics with a transient cell line were expected to deviate from the process parameters in the stable mini-pool (Proc-B) and the single clone cell bank–based (Proc-C) processes. Despite Proc-A using transient cell lines as starting materials, high-quality and consistent JS016 materials from Proc-A were produced, with only subtle differences in N-glycan and CE-SDS fragments observed in the product quality attributes, and may largely be considered comparable to the more mature and stable Proc-B and Proc-C materials. The rapid development of this robust CHO process has manufactured more than 10 lots to satisfy the enormous clinical and emergency use demand in the urgent COVID-19

pandemic crisis. All lots possessed matching primary sequences, secondary and tertiary structures, disulfide bond linkage and PTMs.

Compared with Proc-A samples, about a 0.7% greater level of fragments of Proc-B and Proc-C samples was observed in nrCE-SDS, attributable to the formation of low-level HHL fragments. In addition, about a 0.8% higher level of impurities was observed among Proc-B and Proc-C samples during rCE-SDS. With in-depth peptide mapping analysis, the post-HC, nonreducible peak was elucidated as a thioether bond linking HC and LC between LC Cys 216 and HC Cys 222.

FcγRs are expressed in high abundance in monocytes and have been associated with an antibody-dependent enhancement (ADE) effect following the delivery of vaccines and antibody therapeutics for virus defense and prevention in a manner that may mediate virus infection of normal monocytes and exacerbate the erratic activation of immune cells. The embedded design of a subdued Fc effector function may also

lend protection to patients from undesired ADE effects elicited by therapeutic antibody treatments as observed in the setting of other vaccination-induced antibodies.

Given the limited lot numbers and the 3:3:3 design, this study may not be a fully powered comparability study. However, an in-depth analytical and process comparability study still may indicate the consistent product quality profile and the enhancing process performance, which has empowered the successful advancement of the JS016 program at unprecedented speed to achieve a 4-month DNA-to-IND accomplishment. Such an endeavor not only marks a record for the development for a mAb-based therapeutic but also reflects the cohesiveness and execution efficiency of the organization under global pandemic circumstances. The described novel CMC development strategy was seamlessly coupled with transient pool, mini-pool and single-clone WCB process development, resulting in concurrent preclinical and clinical material supply, which provides a ready-made example of biotherapeutics development in response to the urgent COVID-19 pandemic.

Materials and methods

Materials

Nine lots of JS016 drug substances – three lots of drug substances, each from Proc-A (20 mg/mL), Proc-B (40 mg/mL) and Proc-C (100 mg/mL) – were included in the comparability study.

Transient production (Proc-A)

The CHO cell bank was thawed and expanded sequentially in shake flasks with increasing volume and a 50 L WAVE bioreactor. Once enough cells were obtained, the cells were inoculated into a 200 L production single-use bioreactor (SUB) and cultivated in batch mode for 2 days. The transfection reagent (plasmid and PEI) was then transferred into the 200 L SUB to initiate the production, and cultivated in fed-batch mode for 7–10 days. The cell culture fluid was then clarified with depth filtration and purified with a platform purification process (Protein A affinity chromatography – low pH treatment – cation exchange chromatography – anion exchange chromatography – nanofiltration – Ultrafiltration/diafiltration (UFDF)).

Stable production (Proc-B and Proc-C)

The stable pool (Proc-B) or clonal (Proc-C) cell bank was thawed and expanded sequentially in shaking flasks with increasing volume, a 50 L SUB and 500 L SUB. Once enough cells were obtained, the cells were inoculated into a 2000 L production SUB and cultivated in fed-batch mode for 2 weeks. The cell culture fluid was then clarified with depth filtration and purified with a platform purification process (Protein A affinity chromatography – low pH treatment – cation exchange chromatography – anion exchange chromatography – nanofiltration – UFDF).

Analysis of intact and reduced molecular weights

Protein MW measurements were performed on a Vanquish Flex system (Thermo Fisher Scientific, Waltham, MA, USA) coupled to a Q Exactive Plus mass spectrometer (Thermo Fisher Scientific), with a reversed-phase column (Waters™ BioResolve™ RP mAb polyphenyl column, 450 A, 2.7 μm, 2.1 × 150 mm; Waters Corporation, Milford, MA, USA). The BioPharma Finder 3.2 software (Thermo Fisher Scientific) was used to deconvolute raw mass spectra for MW determination. Dithiothreitol (DTT) was used to reduce antibodies in order to analyze heavy-chain (HC) and light-chain (LC) masses. Peptide N-glycosidase F (PNGase F; New England Biolabs Inc., Ipswich, MA, USA) was used for the deglycosylation of antibodies to detect deglycosylated masses. For intact mass analysis, 1 μg of each sample was injected into the column at 90% mobile phase A (0.08% formic acid (FA) + 0.02% trifluoroacetic acid (TFA) in water) and 10% mobile phase B (0.08% FA + 0.02% TFA in acetonitrile (ACN)). After 2 min, a linear gradient of 10–90% mobile phase B in 7 min was used to elute samples, then maintained for 3 min at 90% mobile phase B. For reduced mass analysis, the elution gradient was kept at 20% mobile phase B for 2 min, followed by at 20–32% mobile phase B for 2 min and 32–37% mobile phase B for 8 min; it was then ramped to 90% within 2 min and maintained there for 3 min. The flow rate was a consistent 0.4 mL/min with the temperature of the column set at 70°C. The typical MS parameters for intact/subunit mass analysis were as follows: positive mode; source voltage, 3.8 kV; and sheath gas, 35; with a scan range of 500–5,000 m/z for intact antibody analysis and that of 500–3,500 m/z for subunit analysis, respectively.

Peptide mapping for sequence confirmation and disulfide structure analysis

Peptide mapping analysis was performed on a Vanquish Flex system coupled to a Q Exactive Plus mass spectrometer (Thermo Fisher Scientific, Waltham, MA, USA). During a complete amino acid sequence analysis by LC-MS/MS, the samples were denatured and reduced in the solution containing 6 M of guanidine hydrochloride and 10 mM of DTT for 30 min at 37°C. Alkylation was performed using 25 mM of iodoacetamide for 30 min at room temperature. Samples were desalted and then digested with trypsin or chymotrypsin (Promega Corporation, Madison, WI, USA). For N-glycosylation site profiling, a 1 μL of PNGase F with a weight ratio of 25:1 (protein:trypsin) (Promega Corporation) was used to digest samples at 37°C for 2 h. Then, a reversed-phase UPLC column (Advanced Bio Peptide Mapping column, 2.7 μm, 2.1 × 150 mm; Agilent Technologies, Santa Clara, CA, USA) was used to separate the digested peptides. Data acquisition for digested peptides was performed with the aforementioned LC-MS/MS system, and 20 μL of each sample was injected onto the column at 99% mobile phase A (0.08% FA + 0.02% TFA in water) and 1% mobile phase B (0.08% FA + 0.02% TFA in ACN). Then, the elution gradient was maintained at 1% mobile phase B for 3 min, followed by at 1–34% mobile phase B for 77 min and 34–50% mobile phase B for 10 min, before being ramped up to 99% within 0.1 min and maintained there for

10 min. The flow rate was a consistent 0.3 mL/min and the column temperature was set at 60°C. For MS data acquisition, the electrospray voltage was 3.8 kV and the capillary temperature was 320°C, respectively. Moreover, the resolution of MS1 was set to 70,000 and the scan range was 200–2,000 m/z, combined with an MIT of 100 ms and AGC threshold of 3e6. The HCD energy for the MS2 ion production was set to 27 with normalization collision energy.

For the analysis of disulfide bonds, the samples were denatured and alkylated in the solution containing 6 M of guanidine hydrochloride and 5 mM of N-ethyl maleimide at 56°C for 30 min. Then, the samples were desalted with ultrafiltration and digested with 50:1 w/w (protein:protease ratio) of Lys-C and trypsin, successively. Following this digestion, the peptide mixture solution was divided into two aliquots, where one portion was incubated with 12.5 mM of TCEP and the other part was incubated with an equal volume of purified water; the two preparations were designated as reduced and non-reduced samples, respectively, to facilitate the identification of disulfide bond–linked peptides. The digested peptides were processed and measured by the same procedures outlined in the peptide mapping analysis. The disulfide-containing peptides were identified with the BioPharma Finder 3.2 software and confirmed by manual inspection of the reduced and non-reduced peptide mapping data.

Glycan mapping

N-glycan mapping was performed with the commercial GlycoWorks RapiFluor-MS N-glycan kit (Waters Corporation). Referring to the manufacturer's manual, the N-glycans of all JS016 lots were processed with sequential enzymatic-release, fluorescent-tag labeling and SPE purification steps. The labeled N-glycans were subject to hydrophilic interaction liquid chromatography (HILIC), which was conducted on a UPLC system (H-class ACQUITY UPLC H-class PLUS Bio; Waters Corporation) equipped with an HILIC column (glycan BEH amide column, 130 Å, 1.7 μm, 2.1 × 150 mm; Waters Corporation). Then, the fluorescence detector was deployed at an excitation wavelength of 265 nm and an emission wavelength of 425 nm to record the eluted glycan peaks. The Empower 3™ software (Waters Corporation) was used to acquire and analyze the HILIC–HPLC data.

Free thiol analysis

The Measure-IT™ thiol assay kit (Thermo Fisher Scientific) was used to evaluate the free thiol (SH) groups in the samples. In this context, a series of Measure-IT™ thiol quantitation standards and samples were prepared and treated with the labeling reagent to facilitate a reaction; a plate reader (SpectraMax M5, excitation/emission wavelength: 490 nm/517 nm; Molecular Devices, San Jose, CA, USA) was then used to detect the fluorescence signal. A linear equation was extrapolated from the nominal quantitation reagent concentrations versus the absorbance standard curve, and the measured absorbance values of the samples were then substituted into the linear equation to calculate the content of free thiol, which was reported using a molar ratio (free SH:IgG ratio, mol/mol).

Isoelectric points

The pI of JS016 antibodies was measured by an imaged capillary focusing method using a Maurice iCIEF system (ProteinSimple, Santa Clara, CA, USA) equipped with a 100-μm inner diameter capillary separation column (Maurice cIEF cartridges; ProteinSimple). Approximately 20 μL of sample (1.0 mg/mL) was mixed with 80 μL of cIEF Master Mix, which was composed of 1% methylcellulose, Pharmalyte 3–10 (GE Healthcare, Chicago, IL, USA), 500 mM arginine (Sigma-Aldrich, St. Louis, MO, USA), pI marker (7.05/9.46) (ProteinSimple) and ultrapure water. Prefocusing for 1 mi at 1,500 V and focusing for 7 min at 3,000 V, respectively, were then completed, and an electropherogram was obtained by full capillary imaging at an UV absorbance wavelength of 280 nm. The pIs of JS016 isoforms were ultimately identified using a linear regression of the bracketing pI marker peaks.

Higher-order structure analysis

Secondary structures of JS016 were assessed by modulation spectroscopy (MMS) (RedShiftBio AQS³pro), which uses a tunable, mid-IR solid-state quantum cascade laser to probe a protein sample in a microfluidic transmission cell of approximately a 22.6-μm path length. All the samples and their corresponding buffer blanks were preloaded in a 24-well plate in a pairwise manner; each sample and buffer were then introduced into the microfluidic transmission cell by compressing air at 5 psi and modulated, passing the path of the laser at a frequency of 1 Hz. About 33 wavenumbers across the amide I-band of protein from 1,714 cm^{-1} to 1,590 cm^{-1} were scanned, and the differential absorbance spectra were obtained. Triplicate measurements were collected for each sample, and the spectra data were analyzed using the AQS³delta software.

CD spectroscopy (Chirascan Plus V100; Applied Photophysics Ltd., Leatherhead, Surrey, UK) was used to evaluate the tertiary structures of JS016. Near-UV CD samples were diluted with formulation buffer to 10 mg/mL, and formulation buffer was used for baseline correction. Near-UV CD spectra were registered from 250 to 340 nm, with path length of 1 nm and scanning speed of 120 nm/min.

Thermal analyses of samples were performed using the MicroCal PEAQ-DSC (MicroCal, LLC, Northhampton, MA, USA). Samples were diluted to 1.0 mg/mL with a formulation buffer. The instrument scanned each sample–buffer pair over the temperature range of 20–110°C at 90°C/h. Subsequent data analysis was performed using the MicroCal PEAQ-DSC software.

Charge variants by cation-exchange HPLC

CEX HPLC was performed on an e2695 HPLC system (Waters Corporation) equipped with a UV detector set at 280 nm and a MabPac SCX-10 column (10 μm, 4.0 × 250 mm; Thermo Fisher Scientific). Samples were diluted to 1.0 mg/mL with mobile phase A (20 mM of MES; pH: 6.0) and treated with 250:1 (v/v) (protein:enzyme) of carboxypeptidase B (1 mg/mL) at 37°C for 1 h. Approximately 100 μL of sample was injected onto the

column at 60% mobile phase A and 40% mobile phase B (20 mM of MES + 100 mM of NaCl; pH: 6.0). After 3 min, the sample was eluted with a linear gradient of 40–80% mobile phase B within 40 min. The LC flow rate was fixed at 1.0 mL/min and the temperature of the column was 40°C.

Size variants by SEC HPLC and reduced and nrCE-SDS

SEC HPLC was performed on an e2695 HPLC system equipped with a UV detector set at 280 nm and an XBridge Protein BEH SEC column (200 Å, 3.5 μm, 7.8 × 300 mm; Waters Corporation). Samples were diluted to 4.0 mg/mL with formulation buffer, and a 25-μL injection volume was adopted. The mobile phase (50 mM of phosphate buffer, 300 mM of Na_2SO_4; pH: 7.0) was achieved at a flow rate of 0.8 mL/min.

Both reduced and non-reduced CE-SDS measurements were performed on a Maurice instrument (ProteinSimple). The sample was diluted with sample buffer (1% SDS, with phosphoric acid–citric acid buffer) to a target concentration of 1.0 mg/mL; then, 95 μL of the mAb solution (1.0 mg/mL) was mixed with either 5 μL of 2-mercaptoethanol (reduced samples) or 0.25 M of N-ethylmaleimide (non-reduced samples), vortexed and incubated at 70°C for 15 min (reduced samples) or 5 min (non-reduced samples). Then the reduced and non-reduced samples were infused into a bare fused silica capillary at 4,600 V for 20 s before being separated at 5,750 V for 30 min (reduced samples) or 40 min (non-reduced samples). Peak detections were monitored by UV absorbance at 220 nm, and peak purity was analyzed with the Compass software for iCE (ProteinSimple).

Process-related impurities

Common process-associated impurities – such as HCPs, residual protein A and residual DNA – may raise concerns regarding impurity-induced immunogenicity and safety. As such, HCPs and residual protein A were measured using enzyme-linked immunosorbent assay (ELISA) by a generic CHO HCP ELISA kit and protein A kit, respectively (both obtained from Cygnus Technologies, Southport, NC, USA). The residual CHO DNA in the JS016 samples was measured by a qPCR assay on a Fast 7500 qPCR system (Thermo Fisher Scientific) following the manufacturer's procedure.

RBD-S1 binding by ELISA and surface plasmon resonance

A solid-phase ELISA was conducted to determine the binding affinity of JS016 to the recombinant RBD-S1 protein of SARS-CoV-2. Recombinant RBD-S1 protein (cat. no. DRA32; Novoprotein Scientific, Summit, NJ, USA) was first coated onto the wells of microtiter ELISA plates; then, a serial dilution of JS016 reference material, control and test samples was added and incubated at 37°C for 1 h. Following a series of washing steps using 1× phosphate-buffered saline, detection antibody, a goat anti-human IgG (Fc-specific) conjugated to horseradish peroxidase (HRP; cat. no. A0170; Sigma-Aldrich) was added to the samples. After a final wash, a substrate/chromogen solution was

added to the wells. The substrate changes color in the presence of HRP in proportion to the amount of JS016 bound to RBD-S1. The colorimetric reaction was stopped with 2.0 M of hydrochloric acid and the degree of absorbance was measured with a microplate reader. After the parallelism of the dose–response curves was evaluated, a four-parameter logistic model fit using the SoftMax Pro software (Molecular Devices) was used to determine the amount of sample binding relative to the reference standard. Findings are indicated as percent relative binding values compared with the reference materials.

The mouse anti-human IgG (Fc) antibody was diluted to 25 μg/mL with a fixation reagent (10 mM of sodium acetate; pH: 5.0). First, the surface of a CM5 chip was activated for 420 s with 400 mM of 1-ethyl-3-(3-dimethylaminopropyl)carbodiimide (EDC) and 100 mM of N-hydrosulfosuccinimide (NHS) at a flow rate of 10 μL/min. Second, 25 μg/mL of mouse anti-human IgG (Fc) antibody was injected into both the reference and experimental channels (FC1, FC2) at a flow rate of 10 μL/min for about 420 s, with a fixed amount of about 9,000–14,000 RU. Finally, the chip was sealed for 420 s with 1 M of ethanolamine at 10 μL/min. The JS016 samples with different expression processes were diluted to 2 μg/mL with the operating reagent, then injected into the experimental channel (FC2) at a flow rate of 10 μL/min to capture about 200 to 300 RU. Notably, the reference channel (FC1) does not need to capture ligands. The SARS-CoV-2 RBD protein was diluted with an operating reagent at twice the ratios of 64 nM, 32 nM, 16 nM, 8 nM, 4 nM, 2 nM and 0 nM. The diluted samples were injected in succession into the experimental channel and reference channel at a flow rate of 30 μL/min for 120 s, then dissociated for 150 s. After each concentration analysis, the chip was regenerated for 30 s with 3 M of magnesium chloride at a flow rate of 20 μL/min to wash off the ligands and the undisintegrated analytes. For the next concentration analysis, the experimental channel needed to recapture the same amount of ligand. The KD value of each sample was calculated using the Biacore T200 analysis software and the reference channel (FC1) was used for background deduction.

RBD ELISA blocking assay

A solid-phase ELISA was conducted to establish blocking to recombinant SARS-CoV-2 RBD-S1. JS016 samples competed with recombinant human ACE-2 (cat. no. C419; Novoprotein Scientific) to bind recombinant RBD-S1 protein (cat. no. DRA32; Novoprotein). Recombinant human ACE-2 was spread onto the wells of microtiter ELISA plates. ACE-2 was incubated with varying concentrations of JS016 reference standard, control and test samples with a constant concentration of RBD-S1. Following washing, goat anti-mouse IgG (Fc Specific) conjugated to HRP (cat. no. A2554; Sigma-Aldrich) was added to determine bound samples. Then, following final washing, a substrate/chromogen solution was added to the wells. The substrate color change in the presence of HRP is in proportion to the amount of RBD-S1 bound to ACE-2. The reaction was stopped with 2.0 M of hydrochloric acid (Sinopharm, Beijing, China), and the absorbance was measured with a microplate

reader. After assessing the parallelism of the dose–response curves, the sample binding relative to the reference standard was determined using a four-parameter logistic model fit using the SoftMax Pro software. All findings were presented as percent blocking values relative to the reference materials.

Neutralization assay

The virus neutralization assay was conducted as follows. Briefly, 100 μL of serial dilutions of human sera or monoclonal antibody preparations were added into 96-well plates. After that, 50 mL of pseudo-virus with a concentration of 1,300 TCID50/mL was added into the plates, followed by incubation at 37°C for 1 h. Afterward, Huh-7 cells were added onto the plates (2×10^4 cells/100 μL cells per well) and incubated at 37°C in a humidified atmosphere with 5% CO_2. Chemiluminescence detection was performed after 24 h of incubation. The Reed–Muench method was adopted to calculate the virus neutralization titer.[20]

Fc receptor and component 1q subcomponent binding by BLI

The Octet Red 96 system and HIS1K biosensors (both FortéBio, Fremont, CA, USA) were used for this analysis. This instrument was used to study the kinetics of samples binding to the Fcγ receptor, including FcRn, FcγRI, FcγRIIa (R176), FcγRIIa (H176), FcγRIIb, FcγRIIIa (V176), FcγRIIIa (F176) and FcγRIIIb by biolayer interferometry (BLI). The assays were performed in solid black 96-well plates (cat. no. 65520; Greiner Bio-One, Monroe, NC, USA) using H1S1K biosensors. All reagents were diluted in assay buffer (i.e., phosphate-buffered saline containing 0.02% Tween-20 and 0.1% IgG-free bovine serum albumin). Human Fcγ receptors were used in the loading steps to bind Fcγ receptors to the surfaces of the H1S1K biosensors. The sensors were then moved to assay buffer wells for baseline generation, followed by test samples. Subsequently, then samples were dipped into assay buffer wells for dissociation. A wild-type antibody known to bind to Fc receptors was used as a positive control to detect binding at the same concentrations. Experimental data were fit with a 1:1 binding model and analyzed with a global or steady-state fitting approach using the Octet RED96e Data Analysis version 12.0 software (FortéBio).

C1q binding by BLI was performed as described above for Fc receptor binding with the following exceptions: test samples were used in the loading step to bind the FAB2G biosensors, followed by an interaction with C1q.

Forced degradation stability

The degradation profiles were detected under the conditions of high temperature (40°C; RH: 60%), light (4,500 ± 500 lux, 25°C; RH: 60%) and dark (25°C; RH: 60%) control. The time points for each treatment were days 0, 5, 15 and 20. Subsequent characterization of the degradation samples was conducted by SEC, CEX, rCE-SDS, nrCE-SDS and potency assays as listed in Supplemental Figure S4.

Abbreviations

ACE2	Angiotensin-converting enzyme 2
BLI	Biolayer interferometry
COVID-19	Coronavirus disease 2019
CDC	Complement-dependent cytotoxicity
CEX HPLC	Cation-exchange high-performance liquid chromatography
C1q	First Subcomponent of the C1 complex
DSC	Differential scanning calorimetry
EDC	1-Ethyl-3-(3-dimethylaminopropyl)carbodiimide
ELISA	Enzyme-linked immunosorbent assay
Fc	Fragment crystallizable
FcγRIa	Fc gamma receptor type Ia
FcγRIIa	Fc gamma receptor type IIa
FcγRIIb	Fc gamma receptor type IIb
FcγRIIIa	Fc gamma receptor Type IIIa
FcγRIIIb	Fc gamma receptor Type IIIb
FcRn	Neonatal Fc receptor
HMW	High molecular weight
HC	Heavy chain
HCD	Host cell DNA
HCP	Host cell protein
HILIC	Hydrophilic interaction liquid chromatography
HPLC	High-performance liquid chromatography
IND	Investigational new drug
iCIEF	Imaged capillary isoelectric focusing
LMW	Low molecular weight
LC-MS/MS	Liquid chromatography–tandem mass spectrometry
LC	Light chain
MMS	Microfluidic modulation spectroscopy
NHS	N-hydrosulfosuccinimide
nrCE-SDS	Non-reduced capillary electrophoresis–sodium dodecyl sulfate
PTM	Post-translational modification
qPCR	Quantitative polymerase chain reaction,
RBD	Receptor-binding domain
rCE-SDS	Reduced capillary electrophoresis–sodium dodecyl sulfate
SARS-CoV-2	Severe acute respiratory syndrome coronavirus 2
SEC HPLC	Size-exclusion high-performance liquid chromatography
SPR	Surface plasmon resonance
UV CD	Ultraviolet circular dichroism
WCB	Working cell bank

Disclosure statement

No potential conflict of interest was reported by the author(s).

References

1. Zhou P, Yang X, Wang X, Hu B, Zhang L, Zhang W, Si H-R, Zhu Y, Li B, Huang C-L, et al. Addendum: a pneumonia outbreak associated with a new coronavirus of probable bat origin. Nature. 2020;588(7836):E6. doi:10.1038/s41586-020-2951-z.

2. Beigel J, Tomashek K, Dodd L, Mehta A, Zingman B, Kalil A, Hohmann E, Chu HY, Luetkemeyer A, Kline S, et al. Remdesivir for the treatment of Covid-19 - final report. N Engl J Med. 2020;383 (19):1813–15. doi:10.1056/NEJMoa2007764.

3. Antwi-Amoabeng D, Kanji Z, Ford B, Beutler B, Riddle M, Siddiqui F. Clinical outcomes in COVID-19 patients treated with tocilizumab: an individual patient data systematic review. J Med Virol. 2020;92(11):2516–22. doi:10.1002/jmv.26038.

4. Hoffmann M, Kleine-Weber H, Schroeder S, Krüger N, Herrler T, Erichsen S, Schiergens TS, Herrler G, Wu N-H, Nitsche A, et al. SARS-CoV-2 cell entry depends on ACE2 and TMPRSS2 and is blocked by a clinically proven protease inhibitor. Cell. 2020;181 (2):271–80.e8. doi:10.1016/j.cell.2020.02.052.

5. Duan K, Liu B, Li C, Zhang H, Yu T, Qu J, Zhou M, Chen L, Meng S, Hu Y, et al. Effectiveness of convalescent plasma therapy in severe COVID-19 patients. Proc Natl Acad Sci U S A. 2020;117 (17):9490–96. doi:10.1073/pnas.2004168117.

6. Cao Y, Su B, Guo X, Sun W, Deng Y, Bao L, Zhu Q, Zhang X, Zheng Y, Geng C, et al. Potent neutralizing antibodies against SARS-CoV-2 identified by high-throughput single-cell sequencing of convalescent patients' B cells. Cell. 2020;182(1):73–84.e16. doi:10.1016/j.cell.2020.05.025.

7. Shi R, Shan C, Duan X, Chen Z, Liu P, Song J, Song T, Bi X, Han C, Wu L, et al. A human neutralizing antibody targets the receptor-binding site of SARS-CoV-2. Nature. 2020;584(7819):120–24. doi:10.1038/s41586-020-2381-y.

8. Zost S, Gilchuk P, Case J, Binshtein E, Chen R, Nkolola J, Schäfer A, Reidy JX, Trivette A, Nargi RS, et al. Potently neutralizing and protective human antibodies against SARS-CoV-2. Nature. 2020;584(7821):443–49. doi:10.1038/s41586-020-2548-6.

9. Yang L, Liu W, Yu X, Wu M, Reichert J, Ho M. COVID-19 antibody therapeutics tracker: a global online database of antibody therapeutics for the prevention and treatment of COVID-19. Antibody Ther. 2020;3(3):205–12. doi:10.1093/abt/tbaa020.

10. Weinreich D, Sivapalasingam S, Norton T, Ali S, Gao H, Bhore R, Musser BJ, Soo Y, Rofail D, Im J, et al. REGN-COV2, a neutralizing antibody cocktail, in outpatients with Covid-19. N Engl J Med. 2021;384(3):238–51. doi:10.1056/NEJMoa2035002.

11. Chen P, Nirula A, Heller B, Gottlieb R, Boscia J, Morris J, Huhn G, Cardona J, Mocherla B, Stosor V, et al. SARS-CoV-2 neutralizing antibody LY-CoV555 in outpatients with Covid-19. N Engl J Med. 2021;384(3):229–37. doi:10.1056/NEJMoa2029849.

12. Bolisetty P, Tremml G, Xu S, Khetan A. Enabling speed to clinic for monoclonal antibody programs using a pool of clones for IND-enabling toxicity studies. mAbs. 2020;12(1):1763727. doi:10.1080/19420862.2020.1763727.

13. Kelley B. Developing therapeutic monoclonal antibodies at pandemic pace. Nat Biotechnol. 2020;38(5):540–45. doi:10.1038/s41587-020-0512-5.

14. Zhang Z, Chen J, Wang J, Gao Q, Ma Z, Xu S, Zhang L, Cai J, Zhou W. Reshaping cell line development and CMC strategy for fast responses to pandemic outbreak. Biotechnol Prog. 2021;37(5):e3186. doi:10.1002/btpr.3186.

15. Ambrogelly A, Gozo S, Katiyar A, Dellatore S, Kune Y, Bhat R, Sun J, Li N, Wang D, Nowak C, et al. Analytical comparability study of recombinant monoclonal antibody therapeutics. mAbs. 2018;10 (4):513–38. doi:10.1080/19420862.2018.1438797.

16. Saunders K. Conceptual approaches to modulating antibody effector functions and circulation half-life. Front Immunol. 2019;10:1296. doi:10.3389/fimmu.2019.01296.

17. Liu L, Wang L, Zonderman J, Rouse J, Kim H. Automated, high-throughput infrared spectroscopy for secondary structure analysis of protein biopharmaceuticals. J Pharm Sci. 2020;109 (10):3223–30. doi:10.1016/j.xphs.2020.07.030.

18. Wen J, Arthur K, Chemmalil L, Muzammil S, Gabrielson J, Jiang Y. Applications of differential scanning calorimetry for thermal stability analysis of proteins: qualification of DSC. J Pharm Sci. 2012;101(3):955–64. doi:10.1002/jps.22820.

19. Yu C, Zhang F, Xu G, Wu G, Wang W, Liu C, Fu Z, Li M, Guo S, Yu X, et al. Analytical similarity of a proposed biosimilar BVZ-BC to bevacizumab. Anal Chem. 2020;92(4):3161–70. doi:10.1021/acs.analchem.9b04871.

20. Li Q, Wu J, Nie J, Zhang L, Hao H, Liu S, Zhao C, Zhang Q, Liu H, Nie L, et al. The impact of mutations in SARS-CoV-2 spike on viral infectivity and antigenicity. Cell. 2020;182(5):1284–94.e9. doi:10.1016/j.cell.2020.07.012.